International Journal of Pressure Vessels and Piping 108-109 (2013) 51–60

Contents lists available at SciVerse ScienceDirect

International Journal of Pressure Vessels and Piping

journal homepage: www.elsevier.com/locate/ijpvp

Effect of different electrode tip angles with tilted torch in stationary gas tungsten arc welding: A 3D simulation

M. Abid [a], S. Parvez [a], D.H. Nash [b,*]

[a] Faculty of Mechanical Engineering, GIK Institute, Topi, KPK, Pakistan
[b] Department of Mechanical Engineering, University of Strathclyde, Glasgow, UK

Keywords:
Gas tungsten arc welding
Welding simulation
Tip angle
Electrode tip
Weld pool
Heat and fluid flow

A B S T R A C T

In this study, the effect of different tip angles (30°, 60°, 90° and 120°) on the arc and weld pool behavior is analyzed in 2 mm and 5 mm arc lengths with tilted (70°) torch. Arc temperature, velocity, current density, heat flux and gas shear are investigated in the arc region and pool convection and puddle shapes are studied in the weld pool region. The arc temperature at the tungsten electrode is found the maximum with sharp tip and decreases as the tip angle increases. The arc temperature on the anode (workpiece) surface becomes concentrated with increase in tip angle. The arc velocity and gas shear stress are observed large with sharp tip and decreasing as the tip angle increases. Current density on the anode surface does not change with tip angle and observed almost the same in all the tip angles in both 2 mm and 5 mm arc lengths. Heat flux due to conduction and convection is observed more sensitive to the tip angle and decreases as the tip angle increases. The electromagnetic force is slightly observed increasing and the buoyancy force is observed slightly decreasing with increase in tip angle. Analyzing each driving force in the weld pool individually shows that the gas drag and Marangoni forces are much stronger than the electromagnetic and buoyancy forces. The weld pool shape is observed wide and shallow in sharp and narrow and deep in large tip angle. Increasing the arc length does not change the weld pool width; however, the weld pool depth significantly changes with arc length and is observed deep in short arc length. The arc properties and weld pool shapes are observed wide ahead of the electrode tip in the weld direction due to 70° torch angle. Good agreement is observed between the numerical and experimental weld pool shapes.

© 2013 Elsevier Ltd. All rights reserved.

1. Introduction

Gas tungsten arc welding process (GTAW) is widely used in the industry to weld large number of metals and alloys with or without the filler material at any position. The torch position plays an important role in determining the weld pool quality. Similarly, different groove geometries (narrow to shallow) are welded effectively by using appropriate electrode tip angle.

Different researchers studied the electrode tip geometry in stationary, axisymmetric GTAW process to investigate the arc and weld pool behavior. Tsai and Kou [1] presented a steady state, two-dimensional model for GTAW to describe heat transfer and fluid flow in the arc produced by the flat and sharpened electrodes. Current density distribution, electromagnetic force, velocity and temperatures were investigated in the arc plasma. It was found that with flat tip, the arc velocity and pressure was low as compared to the sharp tip. The temperature distribution in the arc column was constricted in case of flat tip and it was found that the presence of the gas nozzle did not produce any change in the velocity and temperature distribution. Haidar and Farmer [2] experimentally determined the effect of tip angle on the arc temperatures. For tip angles greater than 60°, the tip area was more uniform and hence the resultant plasma temperatures were more uniformly distributed and found to be less than 60° tip angle. Similarly, for tip angles less than 60°, the heating was more due to the sharp tip area. This heating produced thermionic emission which resulted in a more uniform temperature on sharp tips. The maximum plasma temperatures were therefore found the maximum for 60° tip. Ukita et al. [3] experimentally investigated the effect of tip geometry and torch angle on high speed DCEN TIG welding of ultra-thin aluminum sheets. The tip geometries were conical, conical–spherical and ball end. It was concluded that in ultrahigh speed welding of ultra-thin aluminum sheets, a conical tip angle of 30°, a spherical surface ratio of 25% and a backward inclination angle of

* Corresponding author.
E-mail address: d.nash@strath.ac.uk (D.H. Nash).

0308-0161/$ – see front matter © 2013 Elsevier Ltd. All rights reserved.
http://dx.doi.org/10.1016/j.ijpvp.2013.04.006

Nomenclature

γ	surface tension [N/m]
γ_m	surface tension of iron at T_m [1.943 N/m]
Γ_s	the surface excess at saturation [1.3E−5 mol/m^3]
ϕ	work function [4.3 V]
τ_{Mx}	Marangoni force x-component [Pa]
τ_{My}	Marangoni force y-component [Pa]
ΔH_o	enthalpy of segregation [−1.88E5 J/mol]
A_γ	temperature coefficient of surface tension for iron [4.3E−4 N/m K]
a_i	the activity of sulfur [0.02 wt%]
F	total heat flux [W/m^2]
F_r	radiation flux [W/m^2]
J	current density [A/m^2]
K	adsorption coefficient
k_1	the entropy factor [0.00318 wt%$^{-1}$]
R	gas constant [8.3144 J/mol K]
T	temperature [K]
T_m	melting temperature of iron [1800 K]
V_a	anode fall voltage [2 V]
V_{th}	equivalent volt drop at the anode [1 V]

15° were the most effective welding parameters. The effect of electrode tip angle on arc pressure is studied in Ref. [4]. The pressure found to increase with decrease in tip angle had a peak at 45°. The pressure then decreased with decrease in tip angle. Ushio and Matsuda [5] developed a mathematical model to investigate the welding arc by considering different electrode shapes and turbulent arc flow. The k–ε turbulent model was used in the analysis. The calculated velocity was observed the maximum with sharp electrode tip.

Goodarzi et al. [6] developed a two-dimensional model to study the effect of electrode tip angle on arc by applying the variable cathode surface area surrounded by the arc plasma. The arc was assumed in steady state and the flow was laminar. It was found that increasing the tip angle reduced the span of the arc diameter and increased the current density distribution on the anode surface and hence the heat flux to the anode. The axial velocity in the arc column and gas shear stress on the anode surface was observed to decrease with increase in tip angle. Tanaka et al. [7] experimentally investigated the arc properties such as the current density, arc voltage, heat flux and temperatures for 30°, 45° and 60° tip angles. It was observed that the arc voltage increased as the arc length increased from 2.5 mm to 10 mm. For all the three arc lengths (2.5 mm, 5 mm and 10 mm), the arc temperatures near the cathode tip were found the same in the range of 22,000 K for a 100 A welding current. The change in electrode tip geometry was observed to have insignificant effect on the current density distribution on the anode surface. Another study in Ref. [8] investigated the arc pressure experimentally with 30°, 60° and 90° tip angles and found that the magnitude of the arc pressure is linearly increased with increase in welding current. For a 300 A welding current and 8 mm arc length, the arc pressure was found the maximum with 30° and the minimum with 90° tip angle. Fan and Shi [9] numerically investigated the arc pressure in gas tungsten arc welding. The arc pressure was observed to decrease with increase in tip angle. Mathematical model was developed by Goodarzi et al. [10] to investigate the weld pool with different tip angles. Heat flux, current density and gas shear were calculated from the steady state arc and used as an input to determine the weld pool shape. The author also included the buoyancy and Marangoni effect in the analysis. The fluid flow within the molten weld pool was assumed to be turbulent. The weld pool shapes were determined for a number of electrode tip angles. The results showed that increasing the tip angle increased the depth and decreased the width of the weld pool. The weld pool was observed shallow and wide with sharp and deep and narrow with flat tip.

All the work cited above present two-dimensional axisymmetric models in which the torch is normal to the workpiece. However, the torch is not always normal to the workpiece and can be set to any optimum angle less than 90° to get good quality weld. In this present study, a three dimensional model is presented to investigate the arc and weld pool properties in GTAW with four different tip angles (30°, 60°, 90° and 120°) and two arc lengths (2 mm and 5 mm) with 70° torch angle suggested in Ref. [11]. The study covers the arc properties such as temperature, velocity, pressure, heat flux and gas shear and the weld pool properties such as the electromagnetic, buoyancy and Marangoni forces in the weld pool. The weld pool shape and convection are also analyzed. The model is validated with the experiments and the results are observed in good agreement.

2. Simulation procedure

The GTAW process is simulated using commercial package ANSYS CFX® which uses the Navier–Stokes and Maxwell equations in their conservation form and solves the equations using finite volume method. The governing equations are given in Ref. [12] and will not be presented in this paper. The arc is solved in steady state and the weld pool is calculated in 2 s. Following assumptions are made for the arc;

- The arc is stationary and is in steady state.
- The flow is turbulent.
- The arc is in local thermodynamic equilibrium (LTE).
- The computational domain is in planar symmetry.
- The variable length of the electrode tip surrounded by the plasma is the same for normal (90°) and 70° torch positions.

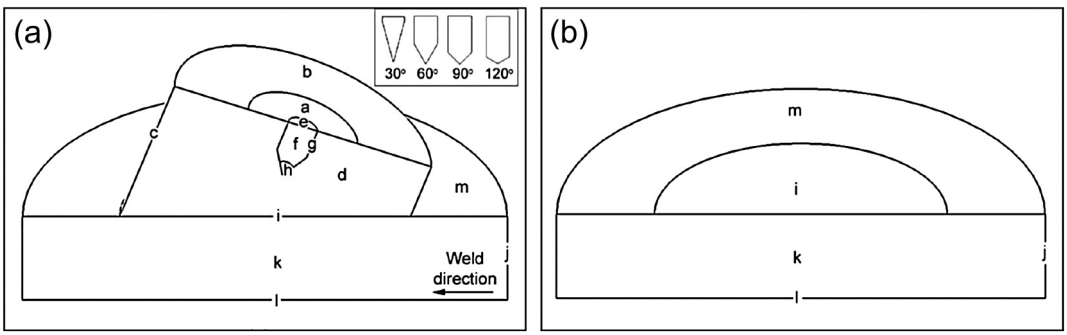

Fig. 1. Computational domain (a) arc; small figure shows the electrode tips (b) weld pool.

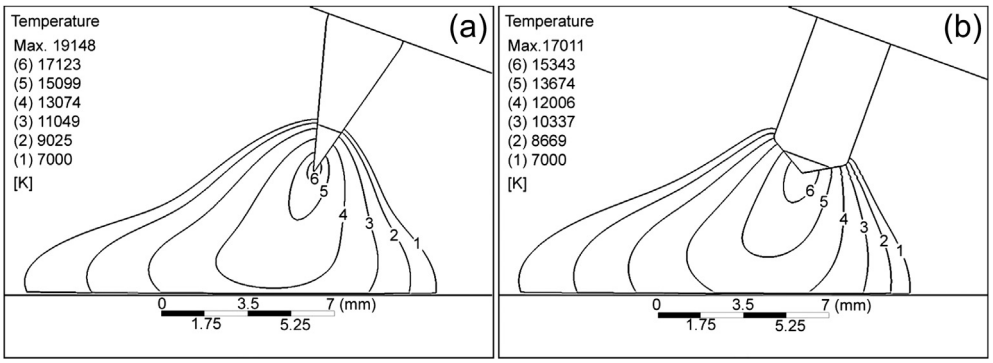

Fig. 2. Temperature profiles in 5 mm arc for tip angles (a) 30°, (b) 120°.

Following assumptions are made for the weld pool;

- The fluid flow is laminar.
- The density variation in the weld pool is very small, Boussinesq approximation is therefore used.
- Heat flux, current density and gas shear for the weld pool are determined in the steady state arc.

2.1. Simulation of the arc

The computational domain for the arc and weld pool calculation is shown in Fig. 1. Due to the 70° torch angle, the geometry becomes planar symmetric. The welding current is 130 A and the power supply is straight polarity DC. The electrode is thoriated tungsten of diameter 3.2 mm. Argon with flow rate of 14 L/min is used as a shielding gas which ionizes at a temperature greater than 7000 K. The plasma is not modeled explicitly rather a simplified approach of increased electrical conductivity is used in the material model to simulation the ionization of argon and formation of the arc plasma. The temperature dependent argon properties are taken from Ref. [13]. A heat source is applied to raise the temperature of the shielding gas up to 12,000 K and once the arc is initiated the heat source is removed. The k–ε model suggested in Ref. [14] is used in the analysis.

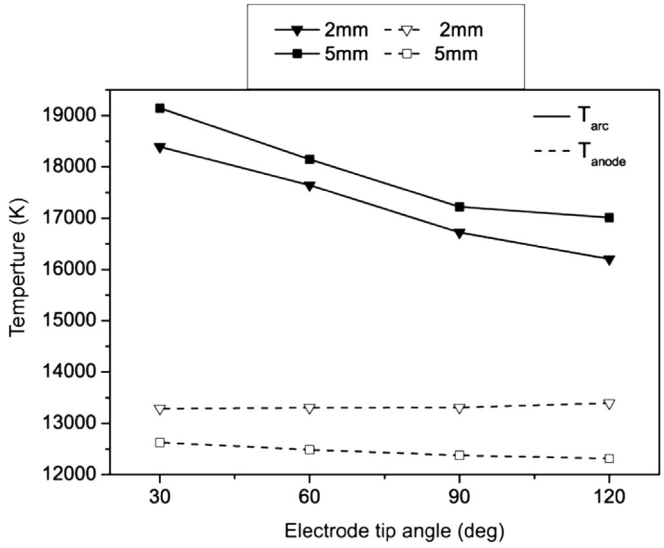

Fig. 3. Maximum arc temperature at the electrode tip and anode surface with different tip angles and 2 mm and 5 mm arc lengths.

The sheath region on the anode (workpiece) surface is also not modeled explicitly and a simplified approach of reference [15] is used to apply the additional heat flux due to electronic contribution on the interface of the arc and weld pool domain (surface i in Fig. 1a). It is found that more than 80% heat is transferred to the workpiece due to the electronic contribution [16]. The remaining heat transfer takes place due to conduction, convection and radiation. Heat transfer due to electronic contribution is determined by three mechanisms, i.e., anode fall, electron potential energy and electron thermal energy given in equation (1) [17].

$$F = J(\phi + V_a + V_{th}) + F_r \tag{1}$$

The values of ϕ, V_a and V_{th} are taken from Ref. [18]. The contribution of radiation flux F_r in the total heat transfer from the arc to the workpiece is only 1.2% [16] and is therefore ignored in this study.

2.2. Simulation of the weld pool

The variation in density of the liquid SS304 is assumed to be small, therefore Boussinesq approximation is used. To simulate the solid and liquid phases of the weld pool, large viscosity of 1E5 cp is defined where the temperature is less than the solidus and actual viscosity is defined where the temperature is above the liquidus

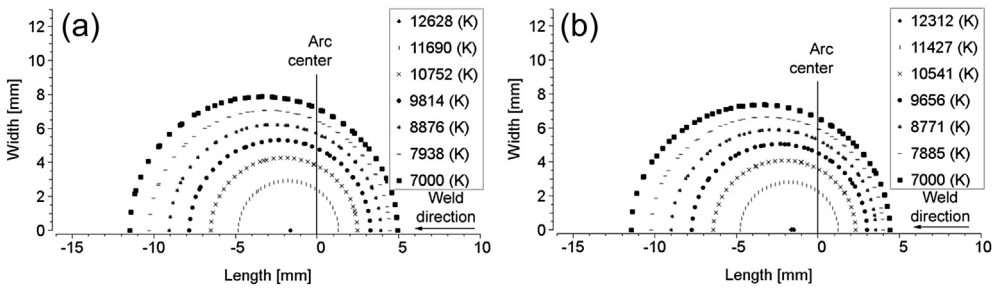

Fig. 4. Temperature distribution on the anode surface in 5 mm arc for tip angles (a) 30°, (b) 120°.

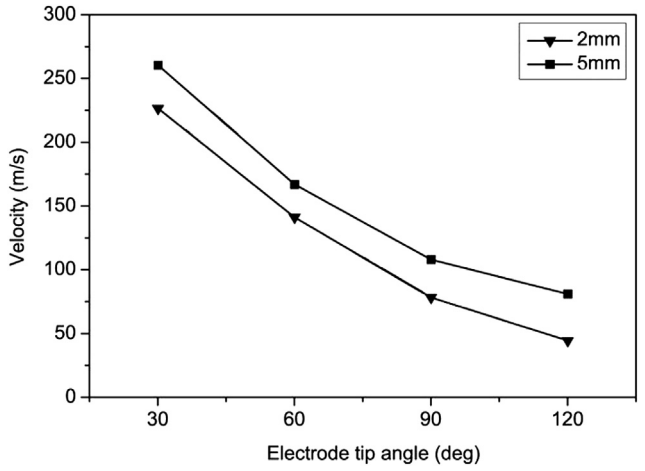

Fig. 5. Maximum arc temperature at the electrode tip and anode surface with different tip angles and 2 mm and 5 mm arc lengths.

temperature of the steel. This method is adapted from Ref. [19]. The workpiece material is SS304, 10 mm in thickness and 50 mm in diameter. Temperature dependent material properties of steel are taken from Ref. [20]. The weld pool is determined by applying the heat flux, current density and gas shear taken from the steady state results of the arc. These results along with the buoyancy and Marangoni forces are used to analyze the weld pool for 2 s. This approach is adopted from Ref. [10].

2.3. Domains and boundary conditions

Boundary details for both the arc and weld pool domains are shown in Fig. 1a and b respectively. In all the cases, a non-uniform hexahedral grid is employed. The grid size is 0.1 × 0.1 mm near and changes to 0.5 × 0.5 mm away from the arc center. The total number of elements in the arc and weld pool domains are 561,660 and 224,790 respectively.

Temperature of the tungsten electrode cannot exceed the melting temperature; it is therefore set to 3000 K. Temperature at *a*, *b*, *c* and *j* boundaries is 303 K. The arc pressure is 1 atm. A current of 130 A is applied on boundary *e* which represents the cross-section of the tungsten electrode. The argon flow is set to 14 L/min at boundary *a* which represents the nozzle outlet. Magnetic induction is zero at boundary *c*. Boundaries *g* and *h* are the fluid and solid interfaces between the electrode tip and the arc domain. To simulate the effect of the electrode tip geometry, variable electrode tip lengths experimentally determined by Haidar and Farmer [2] are used. The part of the electrode tip surrounded by the arc plasma (surface *h* in Fig. 1a) is made conductor and the part which is not surrounded by the arc plasma (surface *g* in Fig. 1a) is made insulator to the current flux. Boundary *i* is the fluid–solid interface between the arc and workpiece regions. The flow through the interfaces is conservative which insures the continuity of heat and current fluxes from one domain to another. Boundaries *d*, *f* and *k* are planar symmetry.

The weld pool is solved separately. A heat transfer coefficient of 20 W/m^2 K is set to boundaries *j*, *l* and *m* of Fig. 1b. Heat flux, current density, gas shear and Marangoni force are applied on surface *i* to calculate the weld pool. The first three boundary conditions are taken from the steady state results of the arc, the last boundary condition is determined according to equation (2) taken from Ref. [21].

$$\tau_{Mx} = \frac{\partial \gamma}{\partial T}\frac{\partial T}{\partial x},\ \tau_{My} = \frac{\partial \gamma}{\partial T}\frac{\partial T}{\partial y} \tag{2}$$

The surface tension of binary mixture of steel is determined according to equation (3), proposed by Sahoo et al. [22];

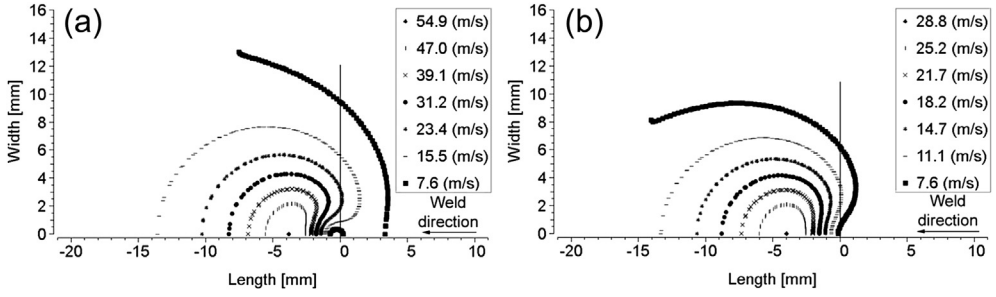

Fig. 6. Velocity distribution on the anode surface in 5 mm arc for tip angles (a) 30°, (b) 120°.

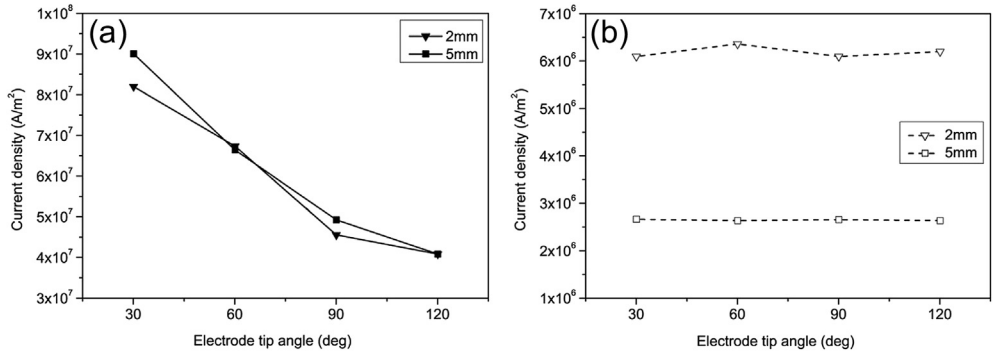

Fig. 7. Maximum current density (a) at the electrode tip, (b) on the anode surface.

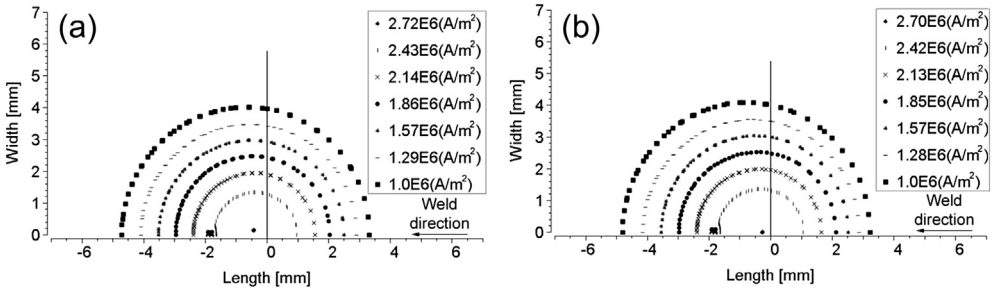

Fig. 8. Current density distribution on the anode surface in 5 mm arc for tip angle (a) 30°, (b) 120°.

$$\gamma(T) = \gamma_m - A_\gamma(T - T_m) - RT\Gamma_s \ln(1 + Ka_i) \quad (3)$$

$$K = k_1 \exp\left(-\frac{\Delta H_o}{RT}\right) \quad (4)$$

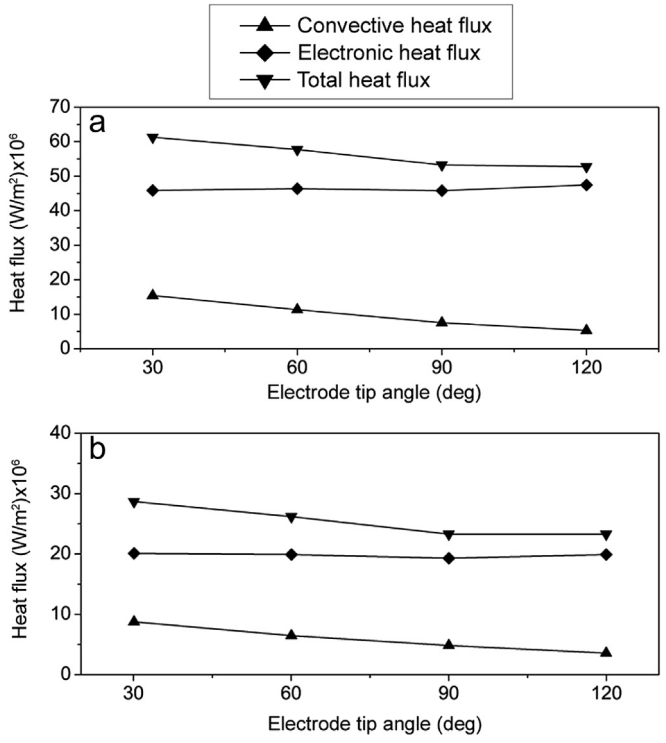

Fig. 9. Heat flux to the workpiece with different tip angles and arc lengths (a) 2 mm, (b) 5 mm.

3. Results discussion

3.1. Arc temperature

Fig. 2 shows typical arc temperatures for the two extreme tip angles (30° and 120°) with 5 mm arc length. The maximum arc temperature at the electrode tip (T_{arc}) and anode (workpiece) surface (T_{anode}) for 2 mm and 5 mm arc lengths are shown in Fig. 3. It is found that the arc temperature near the electrode tip is the maximum (19,148 K) for sharp tip and decreases to 17,011 K as the electrode tip angle increases. It is because sharper electrodes have hotter tips due to the reduced cross-section as compared to the blunt tips. Temperatures are larger in 5 mm as compared to 2 mm arc because the electrical resistance is large in the large arc column which consumes more voltage and consequently the arc temperature increases.

Fig. 4 shows the contours of temperature distribution on the anode surface for 30° and 120° tip angles respectively in 5 mm arc length. The distribution becomes slightly constricted (from 16.5 mm to 16 mm for 7000 K temperature contour) as the electrode tip changes from 30° to 120°. Almost the same decrease in temperature distribution on the anode surface is observed in 2 mm arc length. It is found that the electrode tip angle does not produce any prominent effect on the arc temperature just above the surface of the workpiece. This is shown by T_{anode} in Fig. 3. Increasing the arc length from 2 mm to 5 mm decreases temperature about 7% on the workpiece surface.

3.2. Arc velocity

Maximum arc velocities for different tip angles and arc lengths are shown in Fig. 5. It is found that the maximum arc velocity decreases as the tip angle increases from 30° to 120°. Arc velocity is observed to decrease from 262 m/s to 81 m/s in 5 mm arc and from 228 m/s to 44 m/s in 2 mm arc length. Fig. 6a and b represents the contours of velocity distribution on the anode surface for 30° and 120° tip angles respectively. The minimum velocity contour of

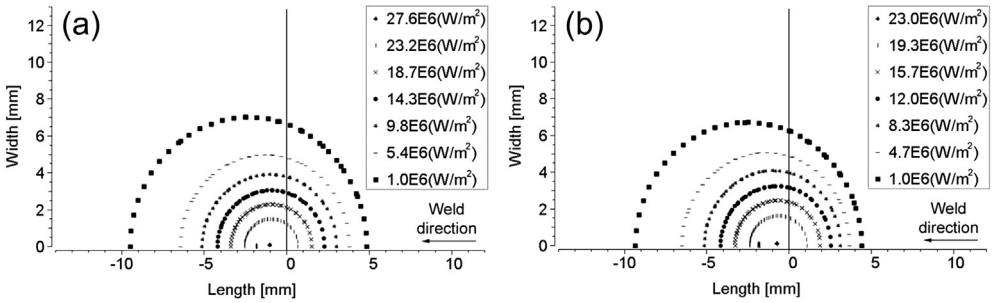

Fig. 10. Heat flux distribution on the workpiece surface in 5 mm arc for tip angles (a) 30°, (b) 120°.

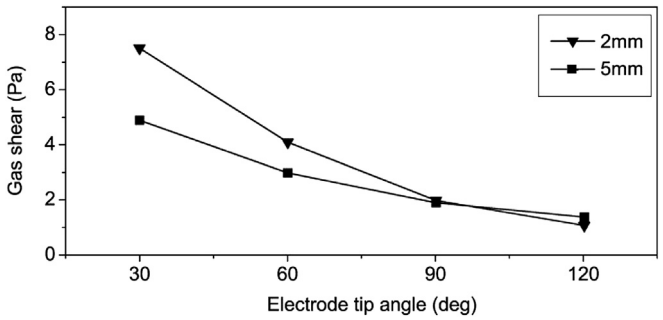

Fig. 11. Maximum gas shear on the workpiece surface with different tip angles.

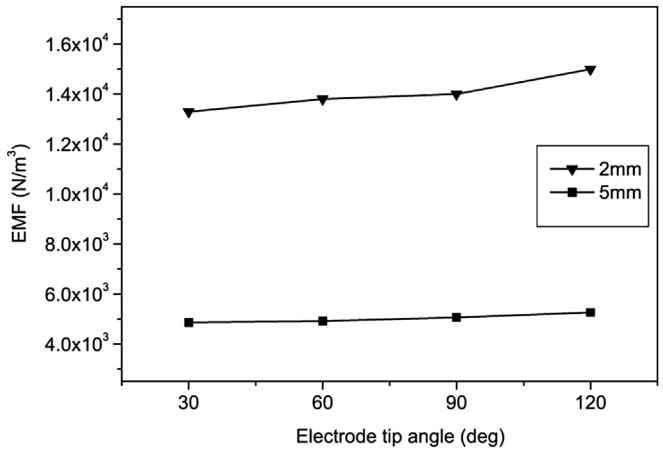

Fig. 12. Maximum electromagnetic force with different tip angles.

7.6 m/s is wider with 30° as compared to 120° tip angle in both 5 mm and 2 mm arc lengths. This phenomenon tends to produce the gas shear on the anode surface which consequently develops wide weld pool with sharp and constricted weld pool with large tip angle.

3.3. Current density

The maximum current density at the electrode tip and on the anode surface for different tip angles is shown in Fig. 7a and b respectively. Current density near the electrode tip is observed sensitive to the tip geometry and decreasing from 9.0E7 A/m^2 to 4.1E7 A/m^2 in 5 mm and from 8.2E7 A/m^2 to 4.1E7 A/m^2 in 2 mm arc length with change in tip angle from 30° to 120°. This decrease is due to the lower electrical potential in the arc with large tip angle. Increasing the arc length decreases the current flux to the workpiece about 57% which results in reduced weld pool size. The electrode tip angle does not produce any dominant change in the current density distribution on the anode surface as shown in Fig. 8.

3.4. Heat flux

Heat flux to the workpiece determines the weld pool. In this study, two sources of heat flux are considered; one is the heat flux due to conduction and convection and the second is due to the electron contribution. It is obvious that the contribution of electronic heat flux is large as compared to the convective heat flux. Total heat flux is the summation of the two sources. As shown in Fig. 9, heat flux due to conduction and convection is more sensitive to the electrode tip angle and decreases from 8.6E6 W/m^2 to 3.4E6 W/m^2 and from 15.4E6 W/m^2 to 5.3E6 W/m^2 with change in tip angle from 30° to 120° in 5 mm and 2 mm arc lengths respectively. Heat flux due to electronic contribution remains unchanged with tip angle and remains almost constant. Total heat flux is therefore affected by the convective heat flux and slightly decreases with increase in tip angle. This trend is observed in good agreement with the two dimensional results of Ref. [6]. Heat flux to the workpiece decreases as the arc length increases from 2 mm to 5 mm. Fig. 10 shows the distribution of total heat flux on the workpiece surface which is observed wide with sharp and constricted with large tip angle.

3.5. Gas shear stress

Fig. 11 represents the maximum gas shear stress on the anode (workpiece) surface with different tip angles and 2 mm and 5 mm arc lengths. The gas shear stress is calculated primarily from the arc velocity and decreasing with increase in tip angle.

The gas shear decreases from 4.9 Pa to 1.4 Pa in 5 mm and from 7.5 Pa to 1.1 Pa in 2 mm arc length when the tip angle changes from 30° to 120°. The gas shear is found almost the same in both the arc lengths when the tip angles are 90° and above. This shows that gas shear is more sensitive to change with the arc length with sharp

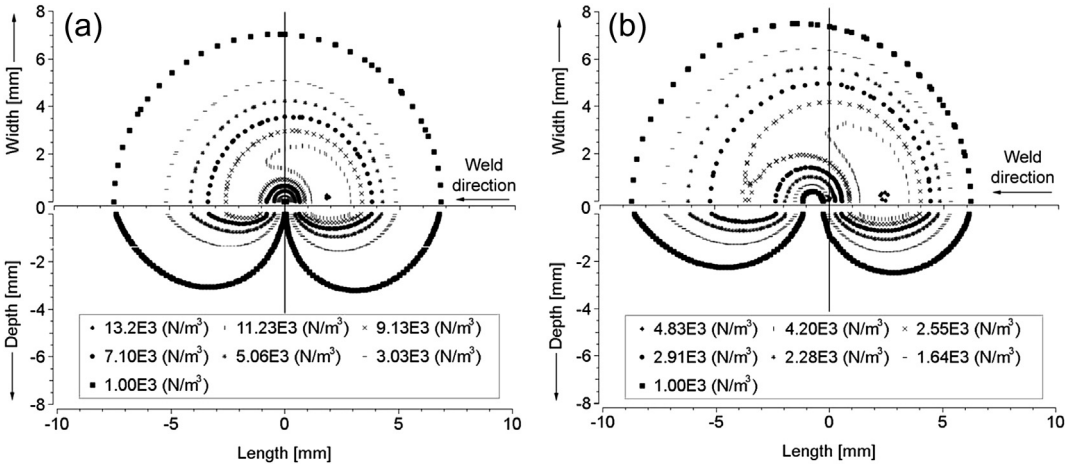

Fig. 13. Electromagnetic force with 30° tip angle and arc lengths (a) 2 mm, (b) 5 mm.

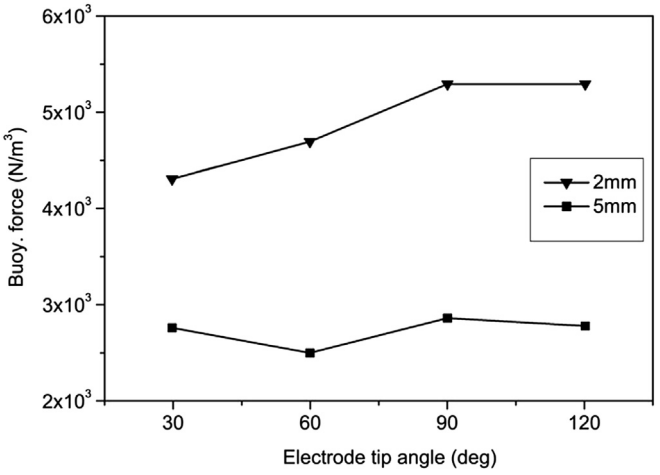

Fig. 14. Maximum buoyancy force with different tip angles.

electrode tip. When heat input is the same to the workpiece, small gas shear tends to enlarge the depth and constrict the width of the weld pool. The weld pool shape is therefore deep and concentrated with large and shallow and wide with small tip angle. Gas shear stress is observed to decrease with increase in arc length from 2 mm to 5 mm.

3.6. Electromagnetic force in the weld pool

The electromagnetic force generates downward pool circulation which increases the weld pool depth; however, this effect is not as dominant as the gas shear and Marangoni convection [10]. The electromagnetic force slightly increases from 4.84E3 N/m^3 to 5.20E3 N/m^3 in 5 mm and from 13.3E3 N/m^3 to 15.0E3 N/m^3 in 2 mm arc length with change in electrode tip from 30° to 120° as shown in Fig. 12.

The distribution of electromagnetic force for 30° tip angle and 2 mm and 5 mm arc lengths is shown in Fig. 13. It is observed that the width of the electromagnetic force does not change significantly; however, the depth increases from 2.5 mm to 3.2 mm as the arc length changes from 5 mm to 2 mm. The weld pool is therefore observed deep in short arc length.

Table 1
Maximum velocity in the weld pool.

	Arc length	Tip angle			
		30°	60°	90°	120°
Velocity (mm/s)	2 mm	157.9	123.8	110.7	113.4
	5 mm	144.8	109.8	70.7	70

3.7. Buoyancy force in the weld pool

Buoyancy force is developed due to the variation in density of molten metal. Buoyancy force produces pool convection which is upward (opposite to the electromagnetic force). Fig. 14 depicts the maximum buoyancy force in the weld pool in all the cases and is observed to decrease with arc length. This decrease is associated with small heat input to the workpiece due to large arc length.

The buoyancy force is found to slightly increase from 2.76E3 N/m^3 to 2.78E3 N/m^3 in 5 mm and from 4.3E3 N/m^3 to 5.3E3 N/m^3 in 2 mm arc length respectively with increase in tip angle; however compared to the gas shear and Marangoni convection, this variation is very small and does not alter the puddle shape. Increasing the arc length from 2 mm to 5 mm decreases the buoyancy force. The effect of electrode tip angle on the distribution of buoyancy force for the two extreme tip angles (30° and 120°) with 5 mm arc length is shown in Fig. 15. The distribution is found different in all the cases and depends on the temperature (to produce density variation) in the weld pool.

3.8. Weld pool convection and shape

The weld pool shape and convection are affected by the electromagnetic, buoyancy, gas drag and Marangoni forces. Although the effect of electromagnetic and buoyancy force is small; however, these still affect the weld pool convection and cannot be ignored in the analysis. Table 1 summarizes the velocities of all the combined driving forces for all the cases.

The Marangoni effect increases with increase in tip angle and the weld pool shape changes from shallow "*w*" to deep "*v*". The weld pool velocity decreases with increase in tip angle and arc length. The weld pool is wide and shallow for 30° and is narrow and deep for 120° tip angle in both 2 mm and 5 mm arc lengths as shown in Fig. 16.

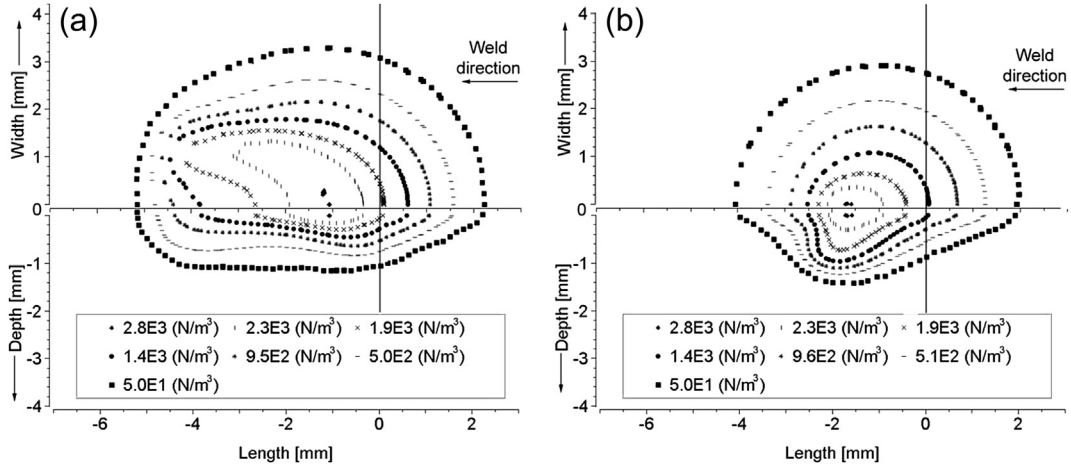

Fig. 15. Buoyancy force in 5 mm arc length for tip angles (a) 30°, (b) 120°.

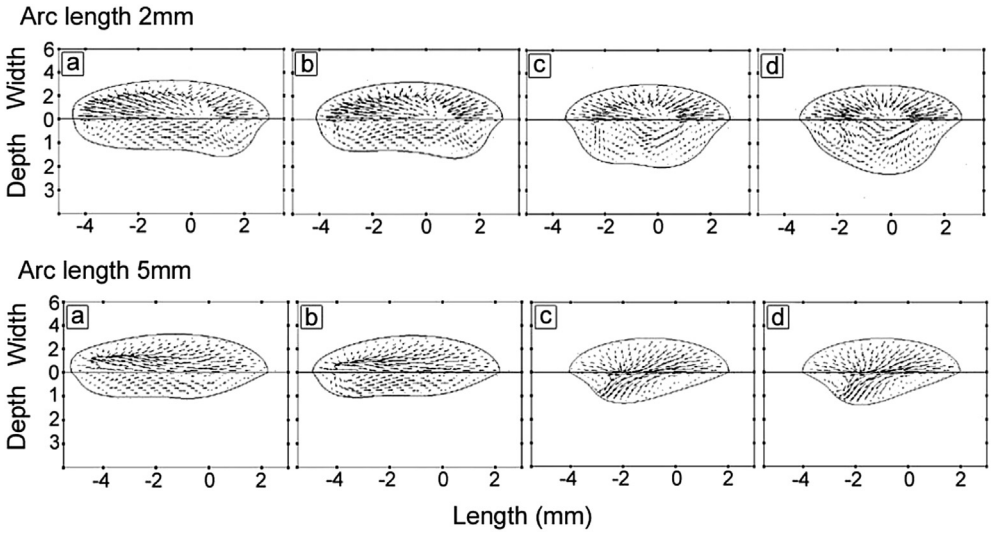

Fig. 16. Weld pool shape and convection for tip angles (a) 30°, (b) 60°, (c) 90°, (d) 120°.

4. Experimental validations

Figs. 18 and 19 show a comparison between the numerical and experimental weld pool shapes for 2 mm and 5 mm arc lengths respectively. The calculated weld pool is about 7.4 mm wide and 1.1 mm deep in 30° and 6 mm wide and 1.5 mm deep in 120° tip angle in 5 mm arc length. Similarly, the weld pool is 7.3 mm wide and 1.5 mm deep in 30° and 6.1 mm wide and 2.2 mm deep in 120° tip angle in 2 mm arc length. It shows that changing the arc length from 5 mm to 2 mm does not alter the pool width significantly. In all the cases, the weld pool is observed wide ahead of the electrode tip due 70° torch angle. Although numerically computed weld pools are observed about 15% large (on average); however, the overall results are observed in good agreement with the experimental results (Fig. 17).

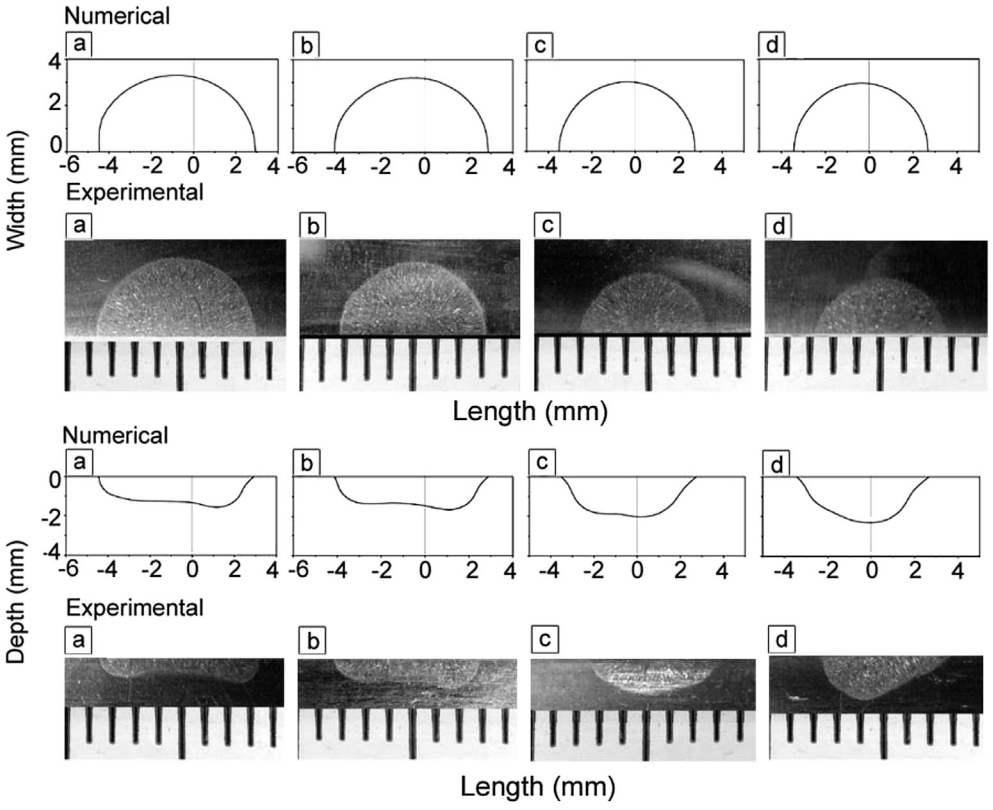

Fig. 17. Numerical and experimental pool shapes in 2 mm arc with tip angle (a) 30°, (b) 60°, (c) 90°, (d) 120°.

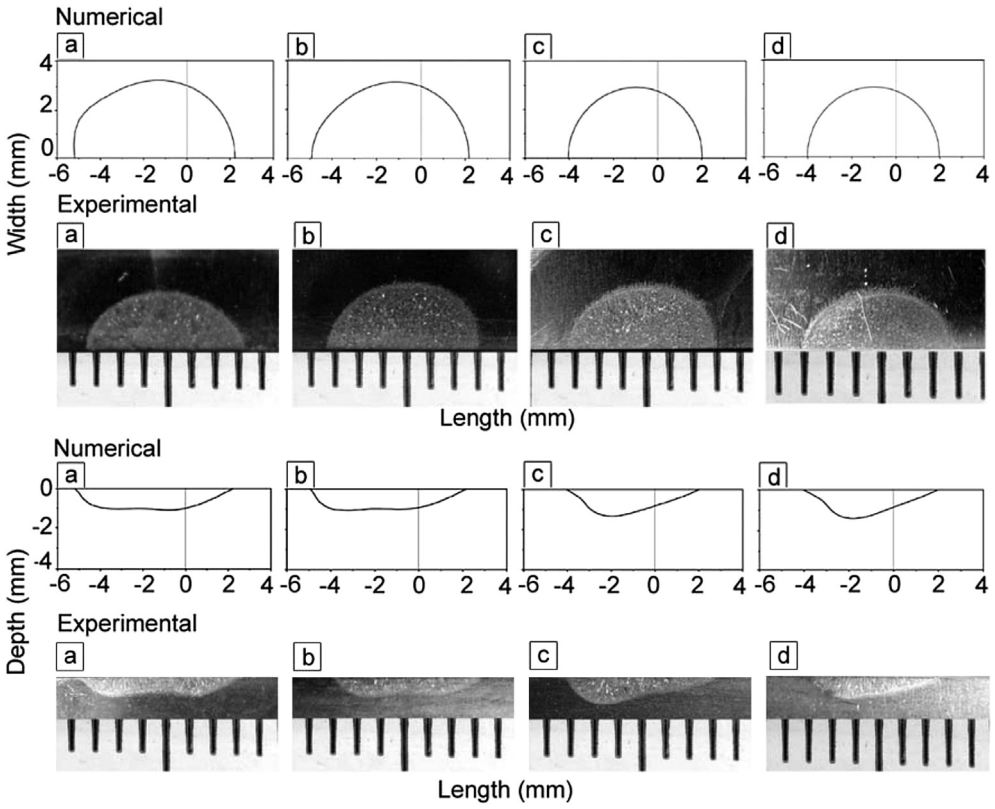

Fig. 18. Numerical and experimental pool shapes in 5 mm arc with tip angle (a) 30°, (b) 60°, (c) 90°, (d) 120°.

5. Conclusions

Four different electrode tips are studied to investigate the effect of tip geometry on arc and weld pool shape. The study also covers two arc lengths of 2 mm and 5 mm with 70° torch angle. The objective is to study the arc and weld pool behavior in stationary GTAW process with tilted torch. Following are the conclusions from the analysis;

- The maximum arc temperature near the electrode tip decreases with increase in tip angle and decrease in arc length. The distribution of the arc temperature is found wide with sharp and concentrated with large tip angle.
- The maximum velocity in the arc column decreases with increase in tip angle. Velocity on the anode surface is observed to decrease with decrease in the arc length from 5 mm to 2 mm.
- The maximum current density at the electrode tip decreases with increase in tip angle. The distribution of current density on the anode surface remains almost the same with tip angles; however, observed to decrease with increase in the arc length.
- Heat flux due to conduction and convection is found more sensitive to the electrode tip geometry and decreases with increase in tip angle. Heat flux due to electronic contribution remains almost unchanged; however, total heat flux is slightly affected by the electrode tip angle. Decreasing the arc length increases heat flux to the workpiece.
- The gas shear decreases as the electrode tip angle increases and is observed more sensitive to the arc length with sharp tip angle.
- The electromagnetic force remains almost the same with tip angles. Changing the arc length from 5 mm to 2 mm reduces the electromagnetic force.
- The buoyancy force is observed to increase with increase in electrode tip angle. Increasing the arc length decreases the buoyancy force in the weld pool.
- Pool convection decreases with increase in tip angle.
- The computed weld pool shapes are observed wide and shallow with small and narrow and deep with large electrode tip angle. The computed pool shapes are compared with the experimental results and are observed in good agreement.

Acknowledgments

The authors are grateful to the ASIA-LINK FastAhead project for financial support for this work under the Contract No. CN/ASIA-LINK/024 (109-093).

References

[1] Tsai MC, Kou Sindo. Heat transfer and fluid flow in welding arcs produced by sharpened and flat electrodes. International Journal of Heat and Mass Transfer 1990;33:2089–98.
[2] Haidar J, Farmer AJD. Large effect of cathode shape on plasma temperature in high-current free-burning arcs. Journal of Physics D: Applied Physics 1994;27:555–60.
[3] Ukita S, Kokubo K, Masuko T. Effects of electrode tip shape and torch angle on high speed DCEN TIG welding. Welding International 2002;16(10):778–83.
[4] Kazuo Hiraoka, Akira Okada, Michio Inagaki. Effect of electrode geometry on maximum arc pressure in gas tungsten arc welding. Journal of the Japan Welding Society 1985;3(2):10–6.
[5] Ushio Masao, Matsuda Fukuhisa. Mathematical modelling of heat transfer of welding arc (part 1). Transactions of JWRI 1982;11(1):7–15.

[6] Goodarzi Massoud, Choo Roland, Toguri James M. The effect of the cathode tip angle on the GTAW arc and weldpool: I. mathematical model of the arc. Journal of Physics D: Applied Physics 1997;30:2744–56.
[7] Tanaka M, Terasaki H, Fujii H, Ushio M, Narita R, Kobayashi K. Anode heat transfer in TIG welding and its effect on the cross-sectional area of weld penetration. Welding International 2006;20(4):268–74.
[8] Lin ML, Eagar TW. Pressure produced by gas tungsten arcs. Metallurgical Transactions B 1986;17B:601–7.
[9] Fan HG, Shi YW. Numerical simulation of the arc pressure in gas tungsten arc welding. Journal of Materials Processing Technology 1996;61:302–8.
[10] Goodarzi Massoud, Choo Roland, Takasu Tomio, Toguri James M. The effect of the cathode tip angle on the gas tungsten arc welding arc and weld pool: II. the mathematical model for the weld pool. Journal of Physics D: Applied Physics 1998;31:569–83.
[11] Miller guidelines for GTAW 2008.
[12] ANSYS CFX®, academic research, release 13.0, help system, ANSYS CFX-solver theory guide. ANSYS, Inc; 2010.
[13] Murphy B, Arundell CJ. Transport coefficients of argon, nitrogen, oxygen, argon-nitrogen, and argon-oxygen plasmas. Plasma Chemistry and Plasma Processing 1994;14:451–90.
[14] Gleizes A, Gonzalez JJ, Freton P. Thermal plasma modeling. Journal of Physics D: Applied Physics 2005;38:R153–83.
[15] Gonzalez JJ, Lago F, Freton P, Masquere M, Franceries X. Numerical modeling of an electric arc and its interaction with the anode: part II. The three-dimensional model-influence of external forces on the arc column. Journal of Physics D: Applied Physics 2005;38:306–18.
[16] Key JF. ASM handbook: welding, brazing and soldering, vol. 6. ASM International; 1993. ISBN: 0871703823.
[17] Lowke JJ, Morrow R, Haidar J. A simplified unified theory of arcs and their electrodes. Journal of Physics D: Applied Physics 1997;30:2033–42.
[18] Quigley MBC, Richards PH, Swift-Hook DT, Gick AEF. Heat flow to the workpiece from a TIG welding arc. Journal of Physics D: Applied Physics 1973;6:2250–8.
[19] Lu Fenggui, Tang Xinhua, Yu Hailiang, Yao Shun. Numerical simulation on interaction between TIG welding arc and weld pool. Computational Materials Science 2006;35:458–65.
[20] Leibowitz L. Properties for LMFBR safety analysis. Technical report. Argonne National Laboratories; 1976. (ANL-CEN-RSD-76–1).
[21] Zacharia T, Eraslan AH, Aidun DK, David SA. Three-dimensional transient model for arc welding process. Metallurgical and Materials Transactions B 1989;20:645–59.
[22] Sahoo P, Debroy T, McNallan MJ. Surface tension of binary metal-surface active solute systems under conditions relevant to welding metallurgy. Metallurgical Transactions B 1988;19B:483–91.